Supporting Information

Synergistic effect of adsorption and electrocatalysis of CoO/NiO heterostructure nanosheet assembled nanocages for high-performance lithium-sulfur batteries†

Longsheng Wu ,[a,b] *Jingping Hu,**[a,b,c] *Xiaorong Yang,*[a,b] *Zhilin Liang,*[a,b] *Sijing Chen,*[a,b] *Lu Liu,*[a,b] *Huijie Hou*[a,b] *and Jiakuan Yang*[a,b,c]

[a] School of Environmental Science and Engineering, Huazhong University of Science and Technology, Wuhan, Hubei, 430074, P.R. China

[b] Hubei Provincial Engineering Laboratory of Solid Waste Treatment, Disposal and Recycling, Wuhan, Hubei, 430074, P.R. China

[c] State Key Laboratory of Coal Combustion, Huazhong University of Science and Technology, Wuhan, Hubei, 430074, P.R. China

Experimental section

Preparation of the CoO/NiO@C-NC or CoO@C-NC modified separator

CoO/NiO@C-NC or CoO@C-NC (4.0 mg), CNTs (2.0 mg), and LA133 (1.0 mg) were added to a mixed solvent of of absolute ethanol and deionized water (20 mL 1:1, v/v), and the mixture was ultrasonically dispersed for 1 h. Then, above mixture was filtered onto the Celgard 2400 membrane, and dried in vacuum at 60 ^{o}C for 12 h. CoO/NiO@C-NC or CoO@C-NC modified separator was obtained by punching the dried modified Celgard 2400 separator into a circular disks of 19 mm in diameter.

Materials characterization

The morphology and structures of the prepared samples were characterized through scanning electron microscopy (SEM, Nova NanoSEM, FEI, Netherlands) and transmission electron microscopy (TEM, Tecnai G2 F30, FEI, Netherlands). The crystal structures of the samples were identified by powder X-ray diffractometer (XRD-7000S, Shimadzu, Japan) at 40 kV and 30 mA with Cu Kα radiation (λ = 0.15406 nm) and a scanning rate of 10° min^{-1} with the 2θ ranging from 5 to 80°. Fourier transform infrared spectroscopy (FTIR) was measured by VERTEX 80 spectrometer (Bruker, Germany). Surface area and pore structure of the samples were characterized using nitrogen adsorption desorption analyzer (ASAP2460, USA) and analyzed with BET isotherm. Surface chemical properties of the samples were analyzed through X-ray photoelectron spectroscopy (XPS, AXIS-ULTRA DLD-600W, Shimadzu, Japan). Thermogravimetry analysis (TGA) was conducted with Diamond TG/DTA thermal analyzer (PerkinElmer, USA) to calculate the sulfur content of prepared samples.

Electrochemical performance tests

Super P/S composite was first prepared to used as the activated material of Li-S batteries through melt-diffusion method. For the preparation of cathode, Super P/S, Super P, and LA133 (8:1:1 by weight) were milled together in deionized water to form uniform slurry. Then, the slurry was coated on the carbon coated Al foil and dried in vacuum at 60 ^{o}C for 12 h. The as-fabricated cathode film was punched into circular disks of 12 mm in diameter. The sulfur mass loading of the electrodes was typically about 1.3~1.4 mg cm^{-2}. Then CR2032-

type coin cells were assembled in an Ar-filled glovebox with H_2O and O_2 concentration below 0.5 ppm. Lithium metal foil was used as the anode and CoO/NiO@C-NC or CoO@C-NC modified Celgard 2400 membrane were used as the separators, respectively. 1.0 M Lithium bis(trifluoromethyl sulfonyl)imide (LiTFSI) dissolved in DOL-DME (1:1, vol) solvent electrolyte with 2.0 wt% $LiNO_3$ was used as the electrolyte, and 30 μL electrolyte was added in each coin cell. The cyclic voltammetry (CV) and electrochemical impedance spectroscopy (EIS) tests were performed with an AUTOLAB electrochemical workstation (PGSTAT302 N, EcoChemie, Netherlands). CV was acquired between 1.7 and 2.8 V, and EIS was measured from 100 mHz to 100 kHz with an amplitude of 5 mV.

Li_2S_6 adsorption tests

Li_2S_6 solution (5 mM) was prepared by dissolving S (4.6 mg) and Li_2S (16.0 mg) in a mixed solvent of DOL/DME (20 mL, 1:1 by volume) and stirring for 12 h at room temperature. Then, 30.0 mg of CoO/NiO@C-NC or CoO@C-NC was added to 5 mL of the above Li_2S_6 solution. The ultraviolet-visible spectra of the Li_2S_6 solution adsorbed by CoO/NiO@C-NC or CoO@C-NC for 24 h were obtained on the UV-6100 spectrophotometer (Mapada, China). All the above operations were carried out in an Ar-filled glove box.

The kinetics evaluation of the polysulfides conversion

The liquid-liquid conversion kinetics of the polysulfides was mainly evaluated by the CV test of symmetrical batteries. CoO/NiO@C-NC or CoO@C-NC (0.040 g), Super P (0.040 g), and polyvinylidene fluoride (PVDF, 0.020 g) were first milled together for 20 min in 1-methyl-2-pyrrolidinone (NMP) solvent to obtain uniform slurry. Then, the slurry was coated on the carbon-coated Al foil and dried in vacuum at 60 ^oC for 12 h, and the as-fabricated dried film was punched into circular disks with 12 mm in diameter. Two identical electrodes were used as the working and counter electrodes with a mass loading of about 1.4 mg cm^{-2} to assemble the CR2032-type coin symmetric cells. In addition, 0.5 M Li_2S_6 electrolyte was prepared by stirring sulfur and Li_2S (5:1 by molar) in the 1.0 M LiTFSI dissolved in DOL/DME (1:1 by volume) at 60 ^oC for 12 h in an Ar-filled glove box, and 30 μL of the Li_2S_6 electrolyte (0.5 M) was used as the cell electrolyte. Celgard 2400 membrane was used

as the separator. CV tests of symmetric cells were measured on the PGSTAT 302N electrochemical workstation with a voltage range of −1.00 to 1.00 V and a scan rate of 1.0 mV s^{-1}.

The liquid-solid conversion kinetics of the polysulfides was mainly evaluated by the Li_2S nucleation measurements. Li_2S_8 electrolyte (0.2 M) was prepared by stirring sulfur and Li_2S (7:1 by molar) in the 1.0 M LiTFSI dissolved in DOL/DME (1:1 by volume) at for 12 h in an Ar-filled glove box. CR2032-type coin cells were assembled with abovementioned CoO/NiO@C-NC or CoO@C-NC electrode and lithium foil as the cathode and anode, and Celgard 2400 membrane as the separator. 15 μL of the Li_2S_8 electrolyte was dropped on to the working electrode side, and 15 μL of the convertional LiTFSI electrolyte was added to the anode side. The cells were discharged to 2.10 V at 0.11 mA, and then kept potentiostatically at 2.09 V for Li_2S to nucleate. The kinetics of the Li_2S dissolution was also conducted by a potentiostatic charge method. The cells were first discharged to 1.70 V at 0.11 mA, and then kept potentiostatically at 2.40 V for Li_2S to dissolve. The nucleation or dissolution capacity of Li_2S was calculated by through Faraday's Law.

Theoretical computation

The adsorption behavior of the polysulfides on the surfaces of different substrate was calculated through Vienna ab initio simulation package (VASP) based on density functional theory (DFT). The 7×7×4 supercell of CoO (200) or NiO (200) with a vacuum layer of 15 Å was used as the substrate, among which the bottom two-layer atoms were fixed and the upper two-layer atoms were relaxed. The projector augmented wave (PAW) pseudo-potential, and Perdew-Burke-Ernzerhof (PBE) exchange correlation function were applied. For the structural optimization, Γ k-points grid was applied as the Brillouin region with the energy cutoff of 550 eV, and the convergence criterion for the energy and maximum force was set to 10^{-5} eV and 0.02 eV/Å, respectively. The adsorption energy (E_{ads}) of the LiPSs on Co (200) or Ni (200) surface were calculated as:

$$E_{ads} = E_{PS\text{-}substrate} - E_{substrate} - E_{PS}$$

where $E_{PS\text{-}substrate}$, $E_{substrate}$, and E_{PS} represent the total energies of the substrate with

polysulfides, the clean substrate, and the polysulfides, respectively.

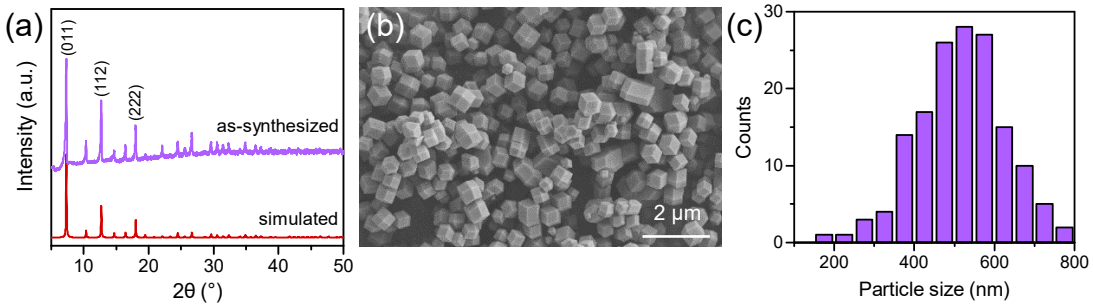

Fig. S1. (a) XRD pattern, (b) SEM image and (c) particle size distribution of the ZIF-67.

ZIF-67 crystal with dodecahedral structure of around 400~600 nm in particle size was synthesized successfully. Three strong diffraction peaks at 2θ of 7.3, 12.7, and 18.0° are observed in the XRD pattern of the as-synthesized ZIF-67, (Fig. S1a), in agreement with the (011), (112), and (222) plane reflections of the simulated sodalite structure and ZIF-67 reported in the literature[1], indicating that the ZIF-67 crystal was synthesized successfully. In addition, the as-synthesized ZIF-67 exhibited a regular dodecahedral structure with the particle size concentrated at 400~600 nm (Fig. S1b and c).

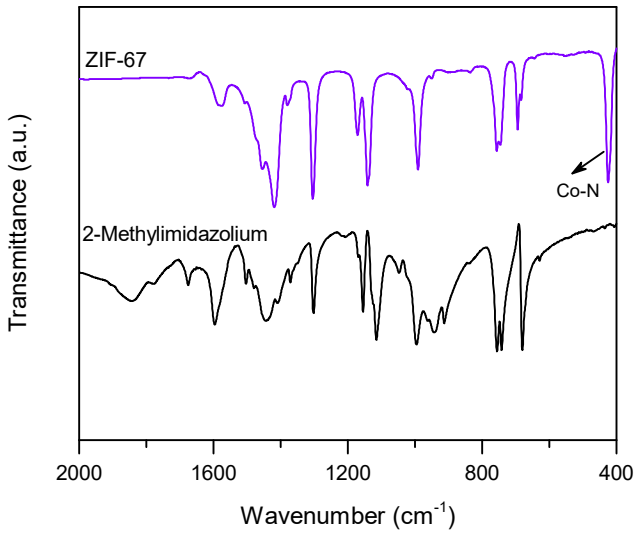

Fig. S2. FTIR spectra of the ZIF-67 and 2-methylimidazolium

Layered double hydroxides were successfully synthesized by etching ZIF-67 with $Ni(NO_3)_2 \cdot 6H_2O$ or $Co(NO_3)_2 \cdot 6H_2O$. The chemical bond and functional group properties of the samples were characterized by FTIR spectroscopy. The peak of the ZIF-67 at 425 cm^{-1} represents the vibration peak of the Co−N bond[2], and most of other peaks were similar to the peaks of 2-methylimidazole, representing the vibration peaks of the imidazole backbone body

in ZIF-67 (Fig. S2). In the FTIR spectra of the NiCo-LDH and Co-LDH, the peaks of the ZIF-67 disappears, and the peaks at 645 cm^{-1}, and in the range of 3000 to 4000 cm^{-1} correspond to the M−OH (M=Ni, Co) bond and -OH group[3], indicating the formation of layered double hydroxides (Fig. S3a). In addition, the peaks of the NiCo-LDH and Co-LDH at 1630, 1502, and 1380 cm^{-1} represent the characteristic peaks of H_2O, $CO_3^{2-}$and NO_3^- of layered double hydroxides (Fig. S3a)[4, 5]. The FTIR spectra of the NiCo-LDH@PDA and Co-LDH@PDA are different from those of NiCo-LDH and Co-LDH (Fig. S3a). The peaks at 1600, 1480, and 1358 cm^{-1} represent the vibration of C=N, C=C, and C-N-C bonds of polydopamine, indicating that polydopamine was successfully coated on the surfaces of Co-LDH and NiCo-LDH[6-8]. However, the peak of the Co-LDH@PDA at 517 cm^{-1} represents the vibration of the O−M−O bonds[9], indicating that Co-LDH may decompose partially during the polydopamine coating process. However, the peak attributed to O-M-O isn't observed in NiCo-LDH@PDA, indicating that $Ni(NO_3)_2{\cdot}6H_2O$ can improve the stability of the NiCo-LDH thus reducing the side reactions during dopamine coating.

The XRD patterns of the prepared samples also prove that layer double hydroxides are synthesized successfully. The diffraction peaks of the Co-LDH and NiCo-LDH at 2θ of 12.3, 25.0, 32.6 and 58.4° represent the (003), (006), (009) and (110) plane reflections of the Co^{2+}/Co^{3+} and Ni^{2+}/Co^{3+} layered double hydroxides[10, 11], and no peak of the ZIF-67 is observed in the XRD patterns of the NiCo-LDH and Co-LDH, demonstrating that ZIF-67 is completely converted into layered double hydroxides (Fig. S3b). Moreover, no peak of polydopamine appears in Co-LDH@PDA and NiCo-LDH@PDA, indicating that dopamine is mainly present in an amorphous state.

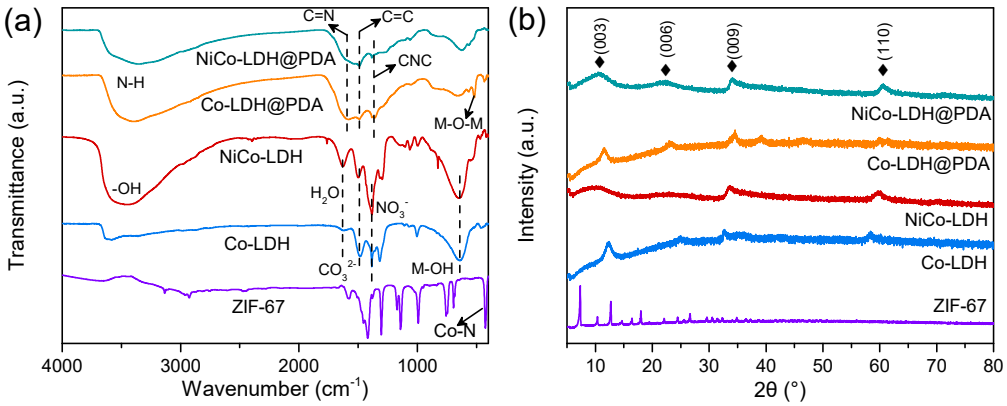

Fig. S3. (a) FTIR spectra and (b) XRD patterns of the ZIF-67, Co-LDH, NiCo-LDH, Co-LDH@PDA and NiCo-LDH@PDA.

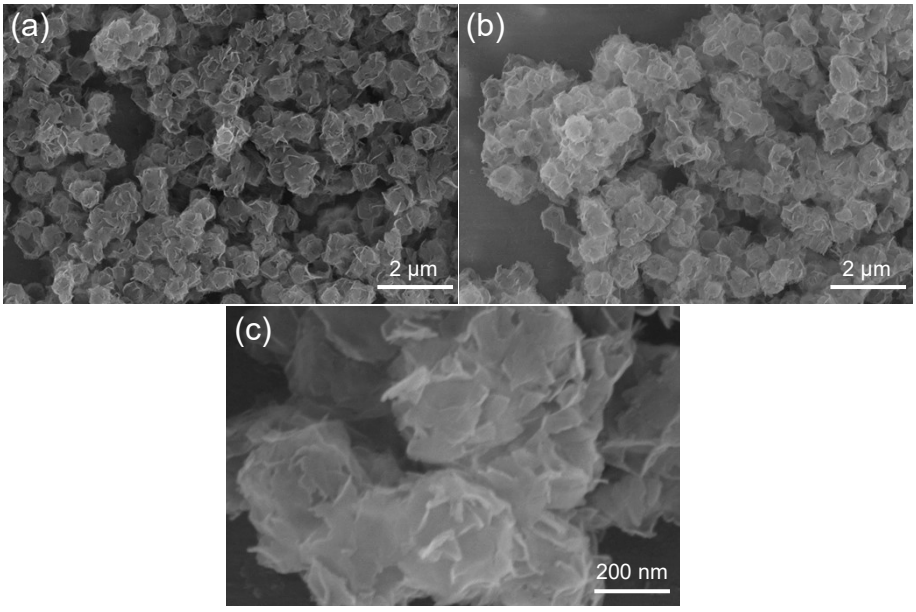

Fig. S4. SEM images of the (a) Co-LDH, (b) Co-LDH@PDA, and (c) CoO@C-NC.

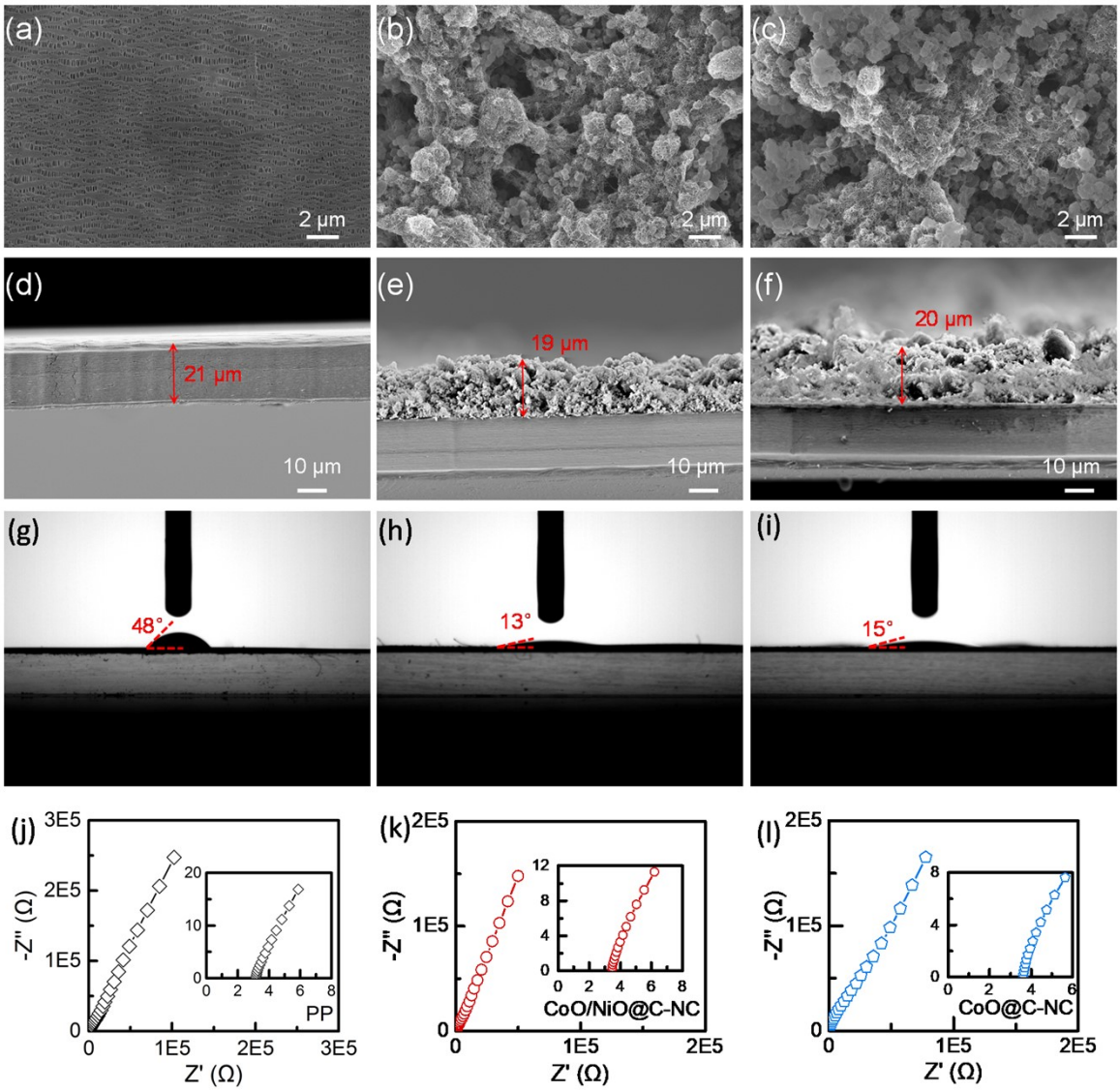

Fig. S5. SEM images of the (a) PP separator, (b) CoO/NiO@C-NC modified separator, and (c) CoO@C-NC modified separator. Cross-section SEM images of (d) PP separator, (c) CoO/NiO@C-NC modified separator, and (f) CoO@C-NC modified separator. Electrolyte contact angle on (g) PP separator, (h) CoO/NiO@C-NC modified separator, and (i) CoO@C-NC modified separator. The Nyquist plots of the stainless steel symmetrical cells with (j) PP separator, (k) CoO/NiO@C-NC modified separator, and (l) CoO@C-NC modified separator.

The ion conductivity of the separator also plays important role in the performance of Li-S batteries. Therefore, EIS tests of the symmetrical cells with different modified separators were performed to evaluate the ion conductivity of different separators according to the equation[12] as:

$$\sigma = l/R_bA$$

where σ represents ion conductivity, l is the thickness of separator, R_b represents the ohmic impedance in the Nyquist plots of different cells, and A represents the area of the stainless steel electrode.

Based one the EIS results, the ion conductivity of the pristine PP separator, CoO/NiO@C-NC modified separator, and CoO@C-NC modified separator are 0.06, 0.11, and 0.10 mS cm^{-1}, respectively.

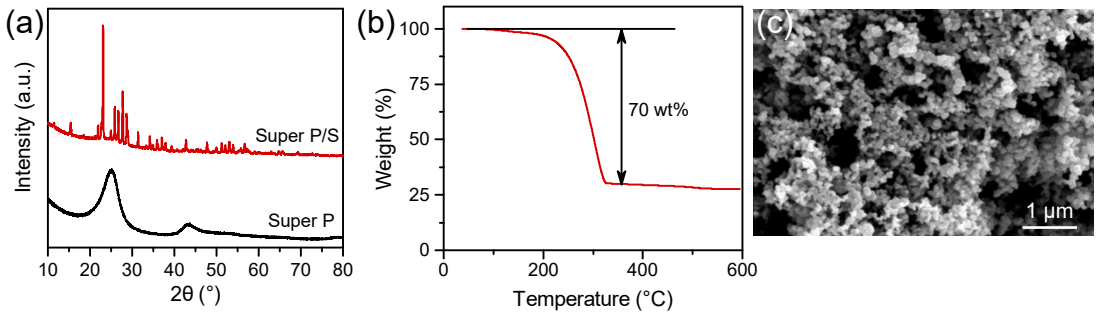

Fig. S6. (a) XRD patterns of the Super P and Super P/S, (b) TGA curve and (c) SEM image of the Super P/S.

The XRD pattern of the Super P shows two characteristic peaks at the 2θ around 25.0 and 43.3°, indicating the graphitization of the Super P. After loaded with sulfur, strong diffraction peaks of sulfur (JCPDS No. 073-5065) appear in the XRD pattern of the Super P/S composite[13], indicating the successful loading of the sulfur (Fig. S6a). The TGA test shows that the sulfur content in Super P/S is about 70.0 wt% (Fig. S6b). The Super P/S exhibits uniform nanoparticle structure and no agglomerated sulfur crystals are observed, indicating that sulfur was uniformly loaded in Super P (Fig. S6c).

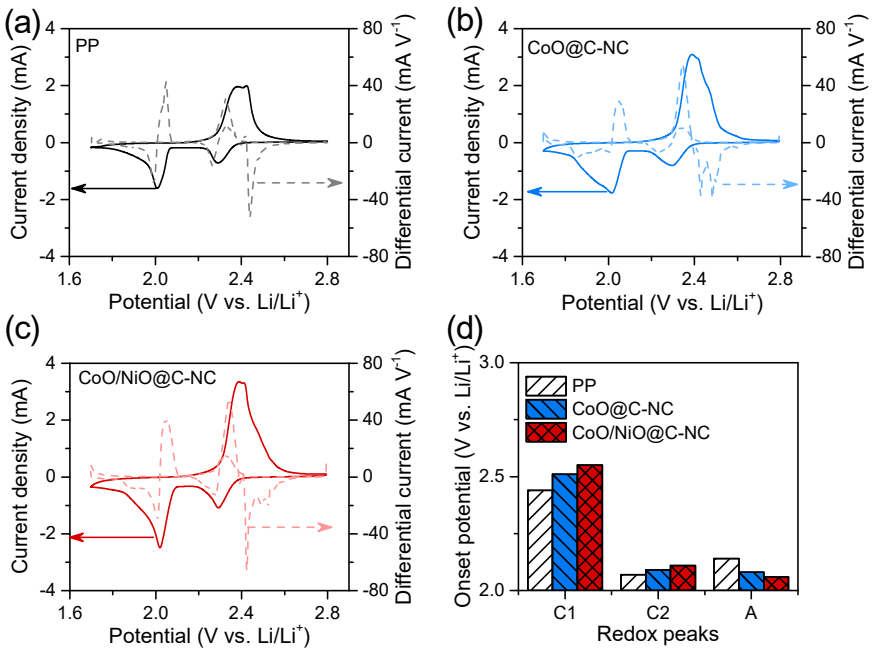

Fig. S7 CV curves and their differential CV curves of the Li-S batteries with different separators: (a) PP separator, (b) CoO@C-NC modified separator, (c) CoO/NiO@C-NC modified separator. (d) Onset potential of the Li-S batteries with different separators.

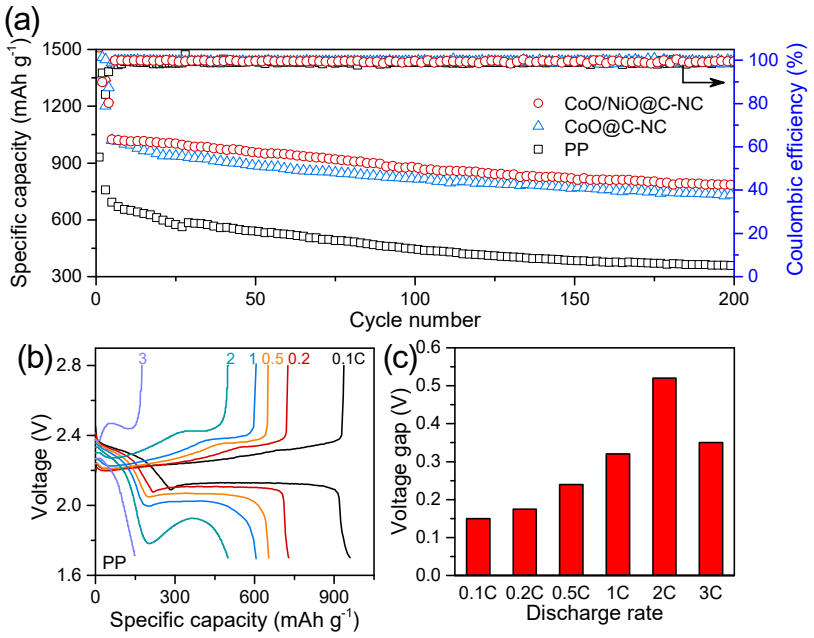

Fig. S8. (a) Cycling performance of the Li-S batteries with CoO/NiO@C-NC, CoO@C-NC modified separator and PP separator at 0.5 C rate. (b) Discharge/charge profiles, and (c) voltage gap between the discharge/charge profiles at different rates of the Li-S battery with PP separator.

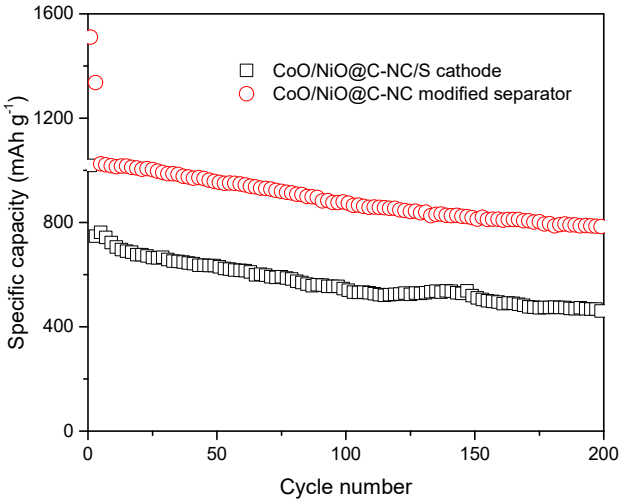

Fig. S9. Cycling performance of the Li-S batteries with CoO/NiO@C-NC as sulfur host and CoO@C-NC modified separator at 0.5 C rate.

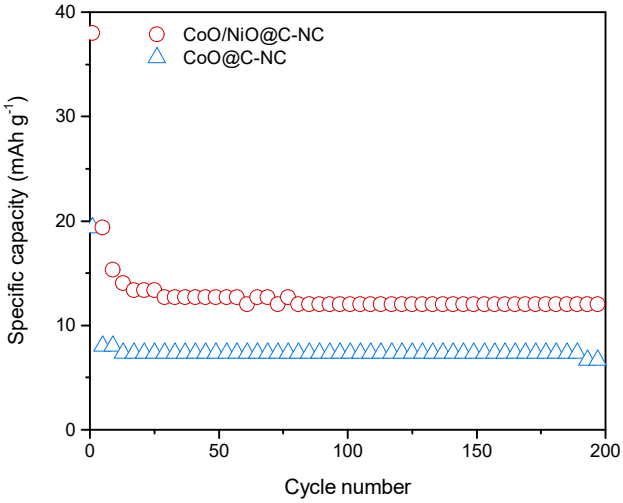

Fig. S10. Cycling performance of the sulfur free batteries with CoO/NiO@C-NC and CoO@C-NC modified separators under 200 mA g^{-1}.

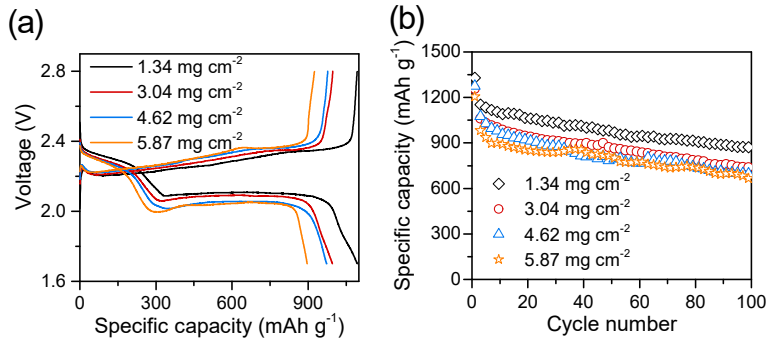

Fig. S11. (a) Discharge/charge profiles, and (b) specific capacity at 0.2 C rate of the Li-S batteries with CoO/NiO@C-NC modified separator at different sulfur loading.

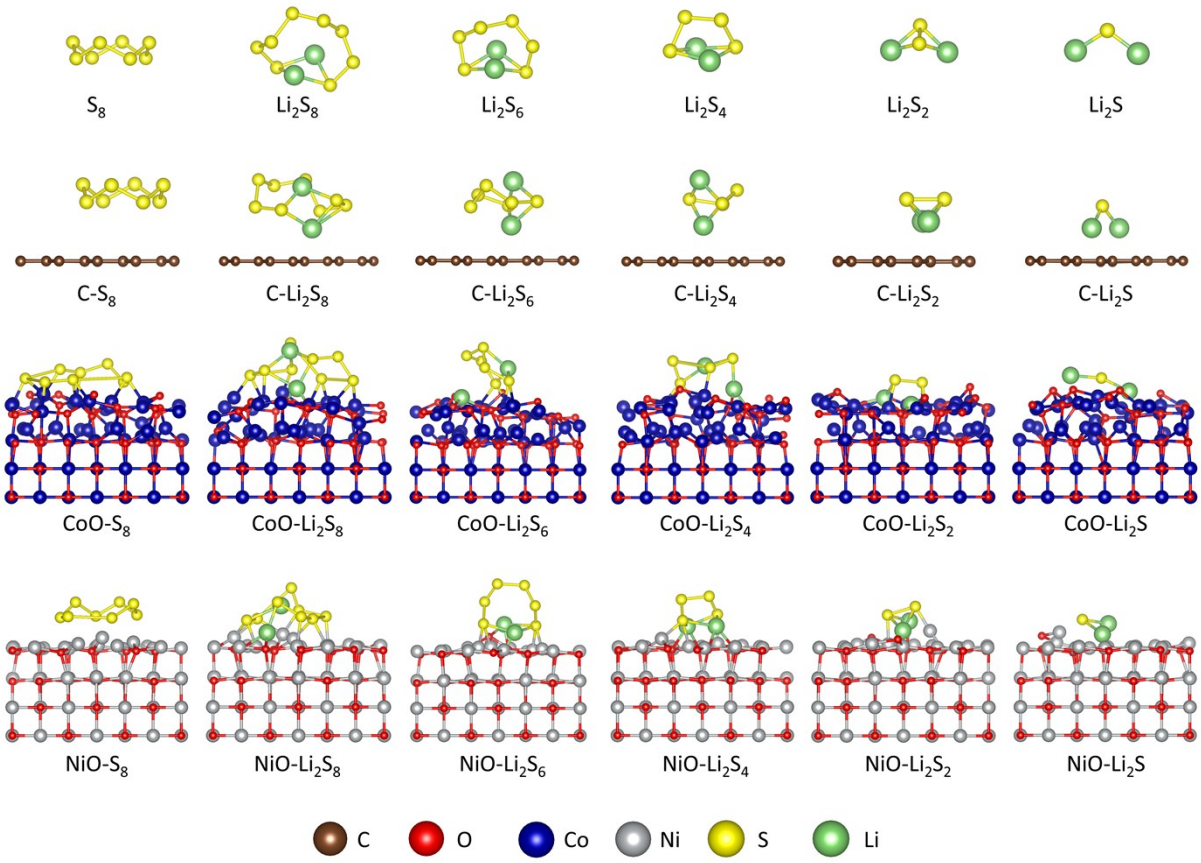

Fig. S12. Optimized geometry configurations of lithium polysulfides on carbon, CoO(200), and NiO(200) planes.

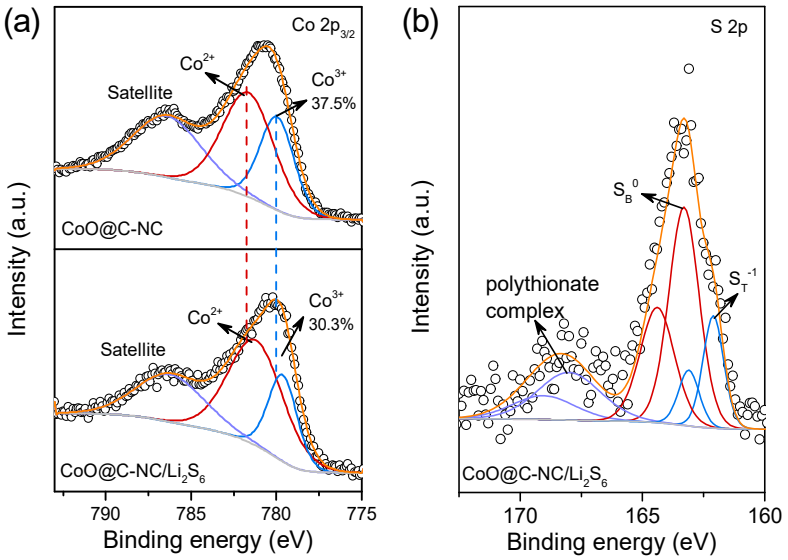

Fig. S13. (a) High resolution XPS spectra of Co $2p_{3/2}$ for CoO@C-NC and CoO@C-NC/Li_2S_6, (b) high resolution XPS spectra of S 2p for CoO@C-NC/Li_2S_6.

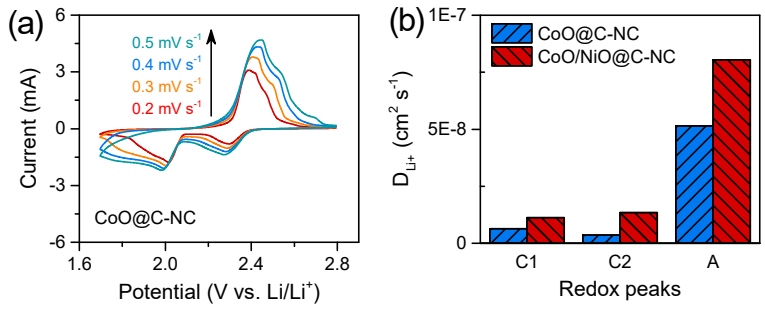

Fig. S14. (a) CV curves of the Li-S battery with CoO@C-NC modified separator at different scan rates, (b) Diffusion coefficient of Li^+ at different redox peaks for the Li-S batteries with CoO@C-NC and CoO/NiO@C-NC modified separators.

Table S1. Electrochemical performance of the Li-S batteries with various modified separators.

Modified materials	Sulfur loading (mg cm^{-2})	Interlayer loading (mg cm^{-2})	Rates/Cycle numbers	Discharge capacity (mAh g^{-1})	Decay rates (%)	References
CoO/NiO@C-NC	1.3	0.63	1C/500	660	0.075%	This work
Nb_2O_5/RGO	1.5	0.10~0.50	0.3C/500	628	0.086%	[14]
Fe_3C/CNF	2.0	0.70~1.00	1C/250	804	0.091%	[15]
Sn/NC	1.3~1.5	0.36~0.43	1C/400	654	0.088%	[16]
Ni/SiO_2/graphene	1.0~1.2	0.24	1C/300	772	0.086%	[17]
Co_3O_4/PI/LLZO	2.5	NA	0.1C/200	630	0.220%	[18]
TiN/NG	1.2	0.50	1C/300	718	0.096%	[19]
CoNi/MPC	1.0~1.5	NA	1C/500	725	0.090%	[20]
Pt/Nb_2O_5/CNTs	1.3~1.5	0.45	0.5C/500	486	0.093%	[21]
NiO/RGO/Sn	4.0	1.40	~0.06C/150	868	0.120%	[22]

Notes: NA means not available

References

1. K. Zhou, B. Mousavi, Z. Luo, S. Phatanasri, S. Chaemchuen and F. Verpoort, *J. Mater. Chem. A*, 2017, **5**, 952-957.
2. F. Cacho-Bailo, I. Matito-Martos, J. Perez-Carbajo, M. Etxeberria-Benavides, O. Karvan, V. Sebastian, S. Calero, C. Tellez and J. Coronas, *Chem. Sci.*, 2017, **8**, 325-333.
3. E. Asadian, S. Shahrokhian and A. Iraji Zad, *J. Electroanal. Chem.*, 2018, **808**, 114-123.
4. X. Ruan, Y. Chen, H. Chen, G. Qian and R. L. Frost, *Chem. Eng. J.*, 2016, **297**, 295-303.
5. X. Wang, S. Yu, Y. Wu, H. Pang, S. Yu, Z. Chen, J. Hou, A. Alsaedi, T. Hayat and S. Wang, *Chem. Eng. J.*, 2018, **342**, 321-330.
6. J. Fu, Z. Chen, M. Wang, S. Liu, J. Zhang, J. Zhang, R. Han and Q. Xu, *Chem. Eng. J.*, 2015, **259**, 53-61.
7. R. A. Zangmeister, T. A. Morris and M. J. Tarlov, *Langmuir*, 2013, **29**, 8619-8628.
8. L. P. Zhu, J. H. Jiang, B. K. Zhu and Y. Y. Xu, *Colloid Surf. B-Biointerfaces*, 2011, **86**, 111-118.
9. A. Sotiles, M. Grassi, M. dos Santos and F. Wypych, *J. Braz. Chem. Soc.*, 2021, **32**, 170-181.
10. Z. Jiang, Z. Li, Z. Qin, H. Sun, X. Jiao and D. Chen, *Nanoscale*, 2013, **5**, 11770-11775.
11. G. Yilmaz, K. M. Yam, C. Zhang, H. J. Fan and G. W. Ho, *Adv. Mater.*, 2017, **29**, 1606814.
12. J.-X. Lin, X.-M. Qu, X.-H. Wu, J. Peng, S.-Y. Zhou, J.-T. Li, Y. Zhou, Y.-X. Mo, M.-J. Ding, L. Huang and S.-G. Sun, *ACS Sustain. Chem. Eng.*, 2021, **9**, 1804-1813.
13. H. Liu, W. Pei, W. H. Lai, Z. Yan, H. Yang, Y. Lei, Y. X. Wang, Q. Gu, S. Zhou, S. Chou, H. K. Liu and S. X. Dou, *ACS Nano*, 2020, **14**, 7259-7268.
14. P. Guo, K. Sun, X. Shang, D. Liu, Y. Wang, Q. Liu, Y. Fu and D. He, *Small*, 2019, **15**, 1902363.
15. K. Wu, Y. Hu, Z. Cheng, P. Pan, M. Zhang, L. Jiang, J. Mao, C. Ni, Y. Zhang, Z. Wang, X. Gu and X. Zhang, *J. Alloy. Compd.*, 2020, **847**, 156443.
16. D. Wang, Q. Cao, B. Jing, X. Wang, T. Huang, P. Zeng, S. Jiang, Q. Zhang and J. Sun, *Chem. Eng. J.*, 2020, **399**, 125723.
17. C. Chen, Q. Jiang, H. Xu, Y. Zhang, B. Zhang, Z. Zhang, Z. Lin and S. Zhang, *Nano Energy*, 2020, **76**, 105033.
18. Zhou, Li, Fang, Zhao, Wang, Zhang and Zhou, *Nanomaterials*, 2019, **9**, 1574.
19. Q. Shen, L. Huang, G. Chen, X. Zhang and Y. Chen, *J. Alloy. Compd.*, 2020, **845**, 155543.
20. R. Luo, Z. Zhang, J. Zhang, B. Xi, F. Tian, W. Chen, J. Feng and S. Xiong, *Small*, 2021, **17**, 2100414.
21. Y. Liu, D. Hong, M. Chen, Z. Su, Y. Gao, Y. Zhang and D. Long, *Chem. Eng. J.*, 2022, **430**, 132714.

22. C. Li, S. Dong, D. Guo, Z. Zhang, M. Wang and L. Yin, *Electrochim. Acta*, 2017, **251**, 43-50.